JOURNAL OF GEOPHYSICAL RESEARCH, VOL. 103, NO. D16, PAGES 19,557–19,567, AUGUST 27, 1998

Radiative effects of sub-mean free path liquid water variability observed in stratiform clouds

Alexander Marshak[1], Anthony Davis[2], Warren Wiscombe, and Robert Cahalan

NASA Goddard Space Flight Center, Climate & Radiation Branch, Greenbelt, Maryland

Abstract. A unique 4-cm-resolution data set of stratocumulus cloud liquid water content (LWC) made possible, for the first time, the generation of credible models of cloud LWC down to centimeter-scales, well below the photon mean free path (mfp) which is typically tens of meters. These models are exploited to study the errors in the usual assumption of LWC homogeneity within three-dimensional (3D) radiative transfer grid boxes, by doing Monte Carlo computations for 30-m cubes resolved down to 10-cm scales. Cloud models with and without vertical variability are compared. We found that vertically homogeneous but horizontally variable cloud structure produces cloud radiation biases of 3-5% relative to the assumption of complete homogeneity. The addition of vertical variability similar to the horizontal variability reduces these biases well below 1%. We therefore conclude that 3D cloud models resolved down to the mfp scale (20-30 m for marine stratocumulus clouds), with an incorrect assumption of homogeneity below that scale are sufficient for modeling radiative properties averaged over mfp and larger scales in both visible and near-infrared spectral regions. This conclusion is restricted to only the overcast cases.

1. Introduction

It is well recognized that any variability of cloud optical depth decreases the domain averaged radiation reflected from clouds; this is a direct consequence of the convexity of the reflectance as a function of optical depth, and it is expressed mathematically as

$$\frac{R(\tau_1) + R(\tau_2)}{2} \le R(\frac{\tau_1+\tau_2}{2}), \qquad (1)$$

where R is reflected radiation and τ is cloud optical depth. For marine stratocumulus (Sc) clouds, the decrease in cloud albedo for a general circulation model (GCM)-scale grid (more than 100 km by 100 km) is around 10-15% [*Cahalan*, 1994; *Chambers et al.*, 1997a; *Barker*, 1996]. For homogeneous clouds to have the same albedo as inhomogeneous ones requires up to a 30% reduction in their cloud liquid water [*Cahalan*, 1994].

The extension of these results to small-scale satellite grids (e.g., 30 m for Landsat) is not obvious, however, because these scales are near the average photon mean free path (mfp) for solar radiation. As a matter of fact, (1) assumes that radiative transfer in each vertical column does not depend on that in other columns [*Cahalan et al.*, 1994]; that is, $R(\tau_1)$ is independent of τ_2. This is of course not valid for small, less than photon mfp, scales where any change of τ_2 will necessary affect $R(\tau_1)$.

As far as we know, there are only a few studies that address the issue of sub-mfp variability in cloud-radiative properties. *Stephens et al.* [1991] and *Davis et al.* [1991a] show that ensemble-averaged direct transmittance deviates from the standard exponential behavior, as already remarked by *Romanova* [1975] for spatial averages. Indeed, the classic derivation of Beer's law explicitly requires extinction to be constant. Conversely, *Davis* [1992] shows that if ensemble-averaged direct transmittance is exponential for all distances, then the medium is necessarily homogeneous. As a result, photon free path is therefore exponentially distributed only in homogeneous media.

More recently, *Knyazikhin et al.* [1998] applied radiative transfer to vegetation canopies with vertical structure simulated by the Cantor set [e.g., *Mandelbrot*, 1977]. They found that as soon as the Cantor-set-like small-scale variability is taken into account, the canopy transmittance no longer follows Beer's law; to force Beer's law to work again, one needs to exponentiate the optical depth by $1/D$ where $D < 1$ [*Mandelbrot*, 1977] is the fractal dimension of the Cantor set.

Turning to multiple scattering, *Cahalan* [1989], *Gabriel et al.* [1990], and *Davis et al.* [1990, 1991a, b] performed numerical and/or analytical computations for cloud systems modeled with singular cascades. In such scale-invariant models, liquid water content (LWC) is concentrated onto a rather sparse subset of space; photons therefore visit many grid cells with small but variable extinction values between two scatterings. In all of these studies strong variability effects were found in the domain-averaged albedo. Ensemble-averaged results using nonfractal Markovian variability models lead to similar conclusions as soon as their parameters are tuned to yield extinction fluctuations at sub-mfp scales [*Avaste and Vainikko*, 1974; *Titov*, 1990; *Malvagi et al.*, 1993; *Byrne et al.*, 1996].

A "mean-field" approach to multiple scattering in media with sub-mfp variability is to use homogeneous plane-parallel theory but without the standard assumption of exponentially

---

[1]Also at Joint Center for Earth Systems Technology (JCET), University of Maryland Baltimore County, Baltimore, Maryland.

[2]Now at Space and Remote Sensing Science Group, Los Alamos National Laboratory, Los Alamos, New Mexico.

Paper number 98JD01728.
0148-0227/98/98JA-01728$09.00

distributed photon free paths. In this spirit, *Barker* [1992] uses an empirical probability density function (pdf) for extinction at each step in a numerical scheme, while *Davis and Marshak* [1997] develop analytically the counterpart of asymptotic ($\tau \gg 1$) theory for Lévy-stable pdfs. Both studies confirm the inequality (1) for domain/ensemble-averaged albedo, and the latter has recently received some experimental validation [*Pfeilsticker*, 1998].

A majority of these investigations of radiative transfer in presence of sub-mfp variability are not grounded in physical reality. Indeed, the technology of cloud liquid LWC measurements [e.g., *Albrecht et al.*, 1988, 1995], plus high aircraft speeds, has prevented spatial resolution of better than 10 m, and most LWC data has a true resolution of no better than 30 m due to inadequate sampling statistics.

Lacking high spatial resolution data, it was necessary to make assumptions. The nearly universal assumption was homogeneity, which creates unnatural scale break in the power spectrum of LWC but which was thought to introduce negligible errors. The opposite assumption is the extreme form of variability; singular (multi)fractal cascades with extreme intermittency lead to significant effects on cloud radiation from sub-mfp variability.

Recent 4-cm resolution measurements of LWC by *Gerber et al.*'s [1994] Particulate Volume Monitor (PVM) allowed us for the first time to asses whether either of these assumptions, complete homogeneity or extreme variability, are useful or whether a better assumption than either is necessary. *Davis et al.* [1998b] applied scale-by-scale analysis to Gerber's data and found a strong centimeter-scale variability, which is consistent with *Baker*'s [1992] earlier findings and the recent report of a strong preferential concentration of cloud droplets by *Shaw et al.* [1998]. *Davis et al.* [1998b] simulated the Gerber probe to see if the centimeter-scale fluctuations were merely an artifact of the finite size of the sampling volume and instrumental filtering and showed that Poissonian noise imposed on a homogeneous background cannot explain the increased variability, which therefore is considered to be physical. This effort makes it possible to generate credible models of cloud LWC all the way down to centimeter-scales, at least for marine Sc.

In this paper, we restrict our focus to single stratus layers, but we justify our models for internal cloud structure with data. More precisely, we exploit our new understanding of sub-mfp LWC variability to study the error in the usual assumption of homogeneity in three-dimensional (3D) radiative transfer grid boxes, by doing Monte Carlo computations for 30-m adjacent cubes, resolved down to 10-cm scales, with LWC modeled according to the results of the Gerber probe analysis. Sections 2 and 3 review the analysis of the high-resolution Gerber probe and indicate ways of generating 3D fractal cloud models based on this data. Section 4 shows the results of radiative transfer calculations for these modeled clouds and compares them with calculations for cloud models that assume homogeneous structure below a photon mfp. In section 5, we discuss our results in the light of a recent study on the general phenomenology of 3D radiative transfer [*Davis et al.*, 1998a]. Concluding statements are made in section 6.

2. Variability in Cloud LWC Data

Analyzing LWC data obtained at an unprecedented 4-cm resolution [*Gerber et al.*, 1994] during the Southern Ocean Cloud Experiment (SOCEX), *Davis et al.* [1998b] discovered a power-spectrum scale-break around 2-5 m (Figure 1). This break separates two distinct scaling regimes: the first from 8 cm (the inverse Nyquist frequency) to about 2-5 m and the second from 2-5 m to about 1 km. Fitting power laws to the two segments of the power spectrum in Figure 1 leads to two scale-invariant regimes:

$$E(k) \propto \begin{cases} k^{-\beta_{small}}, \ \beta_{small}=0.94\pm0.10 & (8\ \text{cm} \le r \le 2\ \text{m}) \\ k^{-\beta_{large}}, \ \beta_{large}=1.62\pm0.07 & (5\ \text{m} \le r \le 1.3\ \text{km}) \end{cases} \quad (2)$$

The scale-break around 2–5 m is robust and appears also in the multifractal statistics such as singular measures and structure functions [*Davis et al.*, 1994, 1998b].

The 1.3-km upper bound is neither statistically nor physically important; it is just the length of the smallest data set analyzed by *Davis et al.* [1998b]. Other cloud LWC data measured during First International Satellite Cloud Climatology Project Regional Experiment (FIRE) [*Albrecht et al.*, 1988] and Atlantic Stratocumulus Transition Experiment (ASTEX) [Albrecht *et al.*, 1995] field programs show a scale-invariant regime from 10-60 m to 30-50 km [*Davis et al.*, 1994, 1996]. The large-scale spectral exponent β_{large} in SOCEX data is in good agreement with spectral exponents in FIRE and ASTEX LWC data.

Since $\beta_{small} \lesssim 1 < \beta_{large}$, the small scales show much more variability than would be obtained merely by extrapolating the large-scale behavior to small scales. This is consistent with *Baker*'s [1992] findings of strong centimeter-scale variability in droplet concentration using a specialized statistical analysis of cloud droplets arrival times in the Forward Scattering Spectrometer Probe (FSSP). Recently, *Shaw et al.* [1998] supported the hypothesis of a highly nonuniform concentration of cloud droplets at centimeter-scales based on the direct numerical simulations.

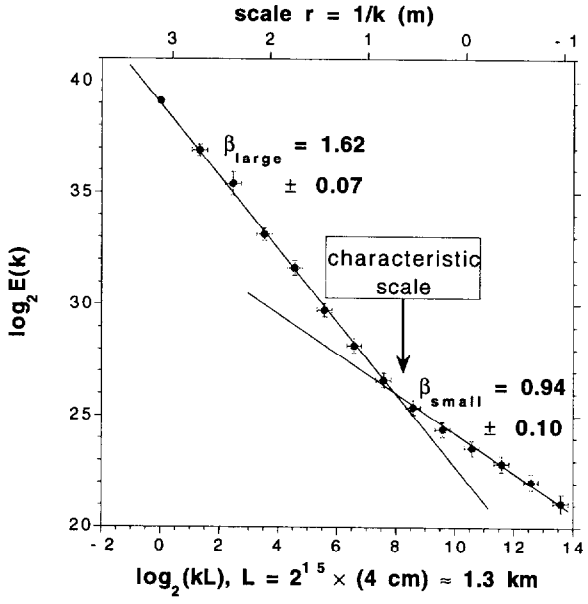

Figure 1. Ensemble-averaged wavenumber spectrum for cloud LWC data measured at 4-cm resolution during the SOCEX field program. The spectral exponent β for each scaling regime is estimated by fitting the ensemble-average $E(k)$ to a power law. The ensemble average is obtained from 37 independent intervals of length 1.3 km (2^{15} points). A scale-break around 2-5 m is indicated.

In general, small-scale fluctuations can be caused by Poissonian noise resulting from the finite sampling volume. To assess this effect on the observed small-scale variability, *Davis et al.* [1998b] simulated stochastically the mechanism for collecting cloud liquid water data by the Gerber probe. They found that Poissonian fluctuations alone are not sufficient to explain the scale-break at 2-5 m and therefore to reject the hypothesis of two distinct scaling regimes. Thus they conclude that the scale-break is more likely to be physical than instrumental; for a more detailed discussion in terms of cloud microphysics, we refer to H. Gerber (Spatial variability of cloud liquid water content, submitted to *Journal of the Atmospheric Sciences*, 1998).

3. Cloud Models

The analysis of cloud LWC variability summarized above makes it possible to build credible cascade models of cloud LWC all the way down to centimeter scales. In this section we first describe general cascades then singular and bounded fractal models emphasizing their wavenumber spectra; finally, a cloud model with two distinct scaling regimes will be developed in one-, two-, and three-dimensional (1D, 2D, and 3D) geometries.

3.1. Cascades in General, Singular, and Bounded Models

Consider the standard cascade model with roots going back to L. F. Richardson [e.g., see *Mandelbrot*, 1977]. Starting with a homogeneous slab, transfer a fraction f_1 of the mass $\langle\varphi\rangle$ from one half to the other in a randomly chosen direction. This is equivalent to multiplying the originally uniform density field on either side by weights $W_1^{(\pm)} = 1\pm f_1$. The same procedure is repeated recursively at ever smaller scales using fractions f_i, multiplying the density at each subinterval by weights $W_i^{(\pm)} = 1\pm f_i$ where $i = 2, 3,\ldots$ is the number of the cascade step. This model is "microcanonically conserved," [*Mandelbrot*, 1974] since at each cascade step the total mass remains unchanged; that is, $(W_i^{(+)} + W_i^{(-)})/2 = 1$.

If we take independently of cascade step i the fractions

$$f_i \equiv 1\text{-}2p, \tag{3a}$$

or equivalently the multiplicative weights

$$W_i^{(\pm)} = W^{(\pm)} = \left\{ \begin{array}{c} 2p \\ 2(1-p) \end{array} \right\} \quad (0 \le p < 1/2), \tag{3b}$$

we have a multifractal "p-model," originally proposed by *Meneveau and Sreenivasan* [1987]. The limit $p \to 1/2$ leads to a constant field, while $p = 0$ corresponds to randomly positioned Dirac δ-functions. So, p directly controls the degree of intermittency. This cascade model is a singular discontinuous one; as $i \to \infty$, $\varphi(x+r)$ decorrelates from $\varphi(x)$ if scale $r \to 0$. As a result, its spectral exponent is always less than 1, namely [*Meneveau and Sreenivasan*, 1987],

$$\beta(p) = 1 - \log_2[1+(1-2p)^2] < 1. \tag{3c}$$

According to (2), this model is an appropriate candidate for the small-scale regime of cloud LWC.

A simple way to obtain $\beta > 1$ is to reduce the variance of the multiplicative weights in (3b) at each cascade step. Taking

$$f_i = (1\text{-}2p)\, 2^{-H(i-1)} \quad (0 \le p < 1/2, H > 0), \tag{4a}$$

or equivalently

$$W_i^{(\pm)} = 1\pm(1\text{-}2p)\, 2^{-H(i-1)} \tag{4b}$$

leads to *Cahalan et al.*'s [1994] "bounded" cascade models. Note that here $f_i \to 0$ ($W_i^{(\pm)} \to 1$) as $i \to \infty$. The limit $H \to \infty$ yields a Heaviside function, a single jump from $2p$ to $2(1-p)$ on the very first cascade step. The limit $H \to 0$ leads back to a singular p-model.

Since at each cascade step of a bounded model the size of the jumps decreases, the bounded model is stochastically continuous; as $i \to \infty$, $\varphi(x+r) \to \varphi(x)$ if $r \to 0$. As a result, its spectral exponent is always larger than 1,

$$\beta(H) = \min\{2H,1\} + 1 > 1, H > 0 \tag{4c}$$

independently of p [*Marshak et al.*, 1994]. Unlike in a p--model, here parameter p controls the variance of the model. Note that in the limiting case of $H = 0$, a bounded model becomes singular, and its spectral exponent is entirely determined by p as in (3c).

3.2. Large- and Small-Scale Cloud Models: A 1D-Case

Equations (4c) and (3c) suggest using bounded cascades to model large-scale fluctuations of LWC and singular cascades for small-scale fluctuations. This would allow us to reproduce the observed power spectrum in (2). As a result, to simulate cloud liquid water, we need four parameters: p_{large} and H_{large} to represent large-scale behavior, p_{small} ($H_{\text{small}} = 0$) to represent small-scale behavior, and, finally, r^*, the characteristic scale separating the two scaling regimes.

Let L be the outer scale of our model and $\langle\sigma\rangle$ be the mean extinction (density). Then the local extinction at scale $r^*=L/2^{n_{\text{large}}}$, the smallest scale of the large-scale fluctuations, is

$$\bar{\sigma}_j = \langle\sigma\rangle \prod_{i=1}^{n_{\text{large}}} W_i^{(\pm)}, \quad j=1,\ldots,2^{n_{\text{large}}}, \tag{5a}$$

where n_{large} is the number of large-scale cascade steps. Since the bounded model is mass conserving, averaging $\bar{\sigma}_j$ at this scale (r^*) gives exactly $\langle\sigma\rangle$,

$$\frac{1}{2^{n_{\text{large}}}} \sum_{j=1}^{2^{n_{\text{large}}}} \bar{\sigma}_j = \langle\sigma\rangle. \tag{5b}$$

The spectral exponent of the large-scale fluctuation is given by (4c) and requires $H = 0.31$ to match the value in (2).

For small scales we use fractal interpolation [*Barnsley*, 1988]. As an interpolator, we choose a simple p-model, which is completely defined by p_{small} and gives us $\beta_{\text{small}} < 1$. We have

$$\sigma_{j_k} = W^{(\pm)n_{\text{small}}}\, \bar{\sigma}_j, \quad j=1,\ldots,2^{n_{\text{large}}}, \quad k=1,\ldots,2^{n_{\text{small}}}, \tag{5c}$$

where σ_{j_k} is the extinction coefficient at scale $r = L/2^{n_{\text{total}}}$ with the total number of cascade steps $n_{\text{total}} = n_{\text{large}}+n_{\text{small}}$, and consequently, the total number of points is $2^{n_{\text{total}}}$.

Figure 2a illustrates the wavenumber spectrum of the above model, where $n_{\text{large}} = 6$ and $n_{\text{small}} = 7$. We clearly see two distinct scaling regimes similar to those in Figure 1. If we set the largest scale $L = 300$ m, then the scale-break $r^* = L/2^{n_{\text{large}}}$

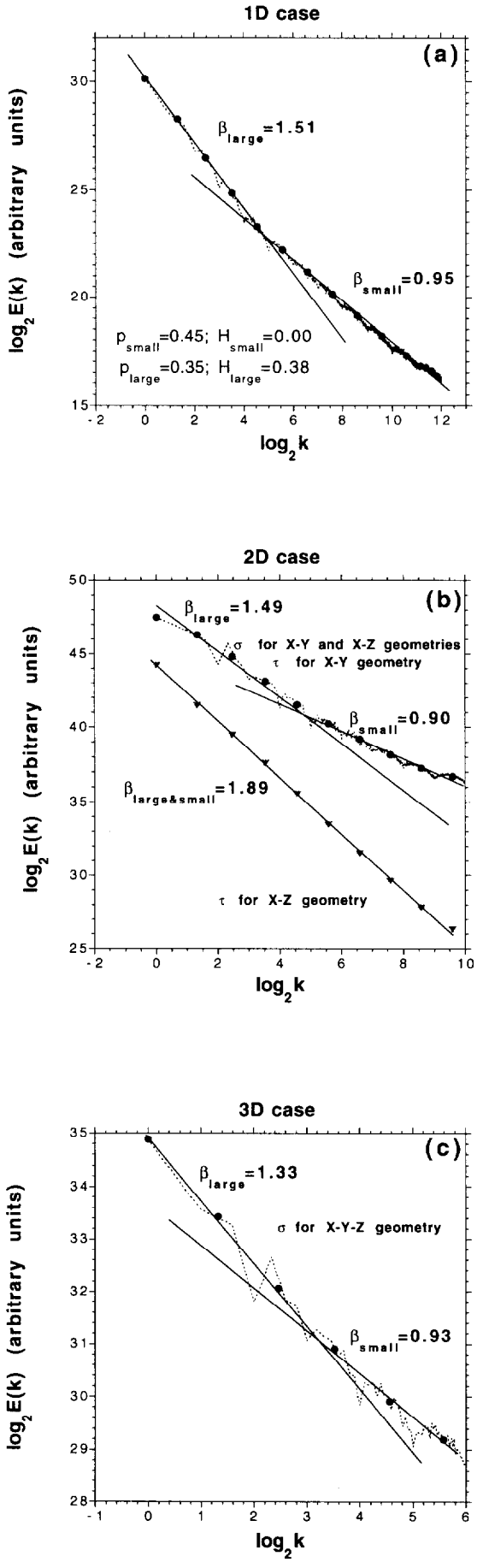

Figure 2. Wavenumber spectrum for cloud cascade models. A large-scale bounded cascade model [*Cahalan*, 1994] with p_{large} = 0.35 and H_{large} = 0.38, then a scale-break to a small-scale p-model [*Meneveau and Sreenivasan*, 1987] with p_{small} = 0.45 is shown. In theory, these values yield $\beta_{large}(H)$ = $\min\{2H, 1\} + 1 = 1.76$ [*Marshak et al.*, 1994] and $\beta_{small}(p)$ = $-\log_2[1-2p(1-p)] = 0.986$, for large and small scales, respectively. However, because of finite number of cascade steps, the numerical values of spectral exponents are smaller. (a) A 13-cascade 1D model averaged over 500 realizations. Large scales are simulated by 6 cascades, small-scales behavior by 7 cascades. (b) An 11-cascade 2D microcanonical model. Large scales are simulated by a 6-cascade 2D bounded model [*Marshak et al.*, 1995a], while small scales are simulated with a 5-cascade 2D p-model. The lowest line is an average over three realizations of the optical depth field defined in (8b). (c) A 7-cascade 3D canonical model. Large scales are simulated with a 3-cascade 3D bounded model, while small scales are simulated with a 4-cascade 3D p-model. Wavenumber spectrum is averaged over 2^7=128 2D fields.

= 4.7 m and the smallest scale $\ell = L/2^{n_{total}}$ = 0.04 m. The parameters remaining to be defined are the mean extinction coefficient $\langle\sigma\rangle$ and geometrical thickness h. We set $\langle\sigma\rangle$ = 43.3 km^{-1} and h = 0.3 km, respectively; these correspond to typical marine Sc clouds with mean optical depth $\langle\tau\rangle$ = 13. Setting $\langle\tau\rangle$ = 13 gives a range of optical depth τ_{j_k} from 2 to 70, while $\overline{\tau}_j$ has a range from 3 to 36; here τ_{j_k} and $\overline{\tau}_j$ are local optical depths at scales $L/2^{n_{total}}$ and $L/2^{n_{large}}$, respectively.

Another characteristic of the optical depth distribution is the gamma function parameter $\nu = \langle\tau\rangle^2/(\langle\tau^2\rangle - \langle\tau\rangle^2)$. It is widely used as a measure of the width of the pdf of τ [*Barker et al.*, 1996]. Our model yields $\nu \approx 3$, while the range of ν for LWC measurements during SOCEX is from 2.3 to 3.9 [*Davis et al.*, 1998b].

To summarize, in this model our clouds are viewed as a vertically homogeneous stratus deck of thickness h where both upper and lower boundaries are horizontal planes. The extinction field depends only on one horizontal coordinate,

$$\sigma(x,y,z) \equiv \sigma(x). \tag{6a}$$

Thus the local optical depth

$$\tau(x,y) = \int_0^h \sigma(x,y,z)dz \equiv h\,\sigma(x) = \tau(x) \tag{6b}$$

also depends only on the x coordinate.

3.3. *Large- and Small-Scale Cloud Models: Two 2D Cases and One 3D Case*

The 2D and 3D cascade models are straightforward generalizations of a 1D model (e.g., see *Marshak et al.* [1995a] for the 2D bounded model details). Similar to the 1D model above, we cascade down to the characteristic scale r^* with parameters p_{large} and H_{large} that represent a bounded cascade model; then we switch to a singular cascade model with p_{small} that corresponds to the small-scale fluctuations of the extinction field.

Cascade models can be [*Mandelbrot*, 1974] either "microcanonical" (if the mean of their weights gives unity for each cascade step and each realization) or "canonical" (if the mean of their weights averaged over many realizations approaches unity). The microcanonical model is quite

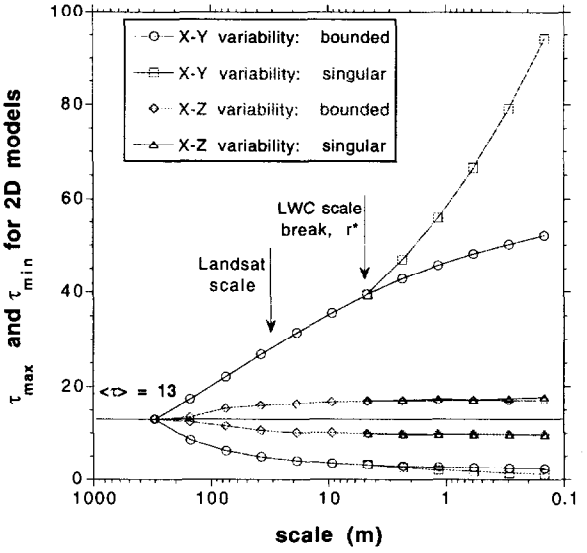

Figure 3. Maximal and minimal optical depths versus scale for 2D cascade models. From 0 (homogeneous case) to 11 cascade steps. Outer curves correspond to x-y variability, while inner curves correspond to x-z variability. At scale r^* (4-5 m), each curve bifurcates into two branches which represent bounded and singular models. Note that optical depth curves for x-z variability defined by (8b) do not distinguish between bounded and singular models. The resolution of Landsat is indicated for comparison.

restrictive, since it forces liquid water conservation at each point in space. Canonical models are less restrictive but only conserve cloud liquid water "in the long run." Figures 2b (upper lines) and 2c illustrate energy spectra of 2D and 3D fields of extinction σ. Here the 2D cascade model was simulated microcanonical, while the 3D one was simulated canonical. Both energy spectra clearly show the scale-break separating two scaling regimes as observed in LWC data and described by (2).

The same 2D cascade model is used to simulate two different extinction fields. The first one is vertically homogeneous with x-y variability; that is,

$$\sigma(x,y,z) \equiv \sigma(x,y) \tag{7a}$$

and

$$\tau(x,y) = \int_0^h \sigma(x,y,z)dz = h\sigma(x,y). \tag{7b}$$

The second model assumes variability in x-z directions,

$$\sigma(x,y,z) \equiv \sigma(x,z); \tag{8a}$$

thus the local optical depth field will vary in only one horizontal direction,

$$\tau(x,y) = \int_0^h \sigma(x,y,z)dz \equiv \int_0^h \sigma(x,z)dz = \tau(x) \tag{8b}$$

Note that the variability of optical depths $\tau(x)$ defined in (6b) and (8b) are completely different. While $\tau(x)$ defined in (6b) has a lognormal-type pdf and a rich structure with an autocorrelation function identical to that of the extinction coefficient, the local optical depth field defined in (8b) is a weakly variable function (see lower curves in Figure 8) with a Gaussian-type pdf. Its wavenumber spectrum is scale-invariant (Figure 2b) with spectral exponent $\beta_{large\&small} > \beta_{large}$; this is another indication on the weaker variability of τ-fields in x-z geometry than in x-y one. For the multifractal properties of these models, see *Naud et al.* [1996].

To illustrate the range of optical depth for both 2D models, in Figure 3 we plotted τ_{max} and τ_{min} of both τ-fields defined by (7b) and (8b), respectively. With 11 cascade steps, the range of scale varies from L = 300 m down to ℓ = 15 cm. For x-y variability, we clearly see the effect of the scale-break at 4-5 m, while the range of optical depth for x-z variability remains almost unchanged. As expected from (3b) and (4b) for x-y geometry, a singular model, as an interpolator, substantially increases τ_{max} and only slightly decreases τ_{min}. In contrast to the integration (7b), which is just the product of extinction $\sigma(x,y)$ and h, the integration (8b) substantially tames the variability of $\sigma(x,z)$; the range of τ (dependent on realization) is, on average, between 9 and 18.

The 3D model has similar scaling properties to that with x-z variability; its 2D optical depth field

$$\tau(x,y) = \int_0^h \sigma(x,y,z)dz \tag{9}$$

is a weakly variable with no scale-break.

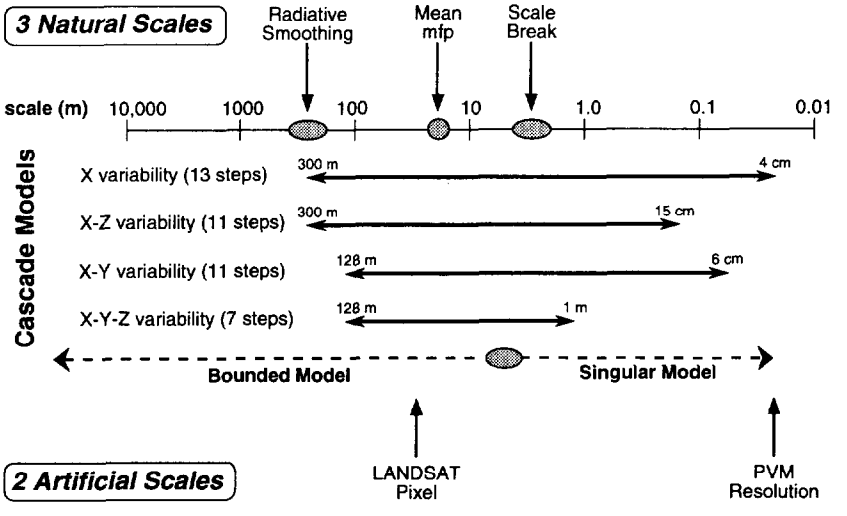

Figure 4. Cascade models and characteristic scales. See text for explanations.

3.4. *Discussion of Models*

Altogether we have four cloud models; each of them has extinction energy spectra similar to those of LWC measured during the SOCEX field program. However, the properties of the corresponding optical depth fields are quite different. While the extinction fields with no vertical variability (x and x-y geometries) have optical depth fields similar to those of extinction, the x-z and x-y-z geometries produce less variable optical depths. As a result, these two classes of models (with and without vertical variability) represent extreme cases rather than a realistic structure of cloud liquid water. Unfortunately, no data of small-scale variability of optical depth to check the validity of our models are expected in the near future. It is very likely that the real cloud structure is somewhere between these two extreme cases but closer to the cases with vertical fluctuations (for x-z extinction fields retrieved from the combined microwave radiometer and millimeter-wave radar measurements, see *Zuidema and Evans* [1998]).

Figure 4 schematically summarizes all four cloud models; number of cascade steps and scale ranges are added for convenience. Three natural and two artificial scales are indicated. For typical marine Sc ($\langle\tau\rangle = 13$ and $h = 300$ m), the natural scales are radiative smoothing scale $(3h/\langle\tau\rangle)^{1/2} \approx$ 200--300 m [*Marshak et al*, 1995b]), mean mfp ($h/\langle\tau\rangle \approx$ 20-30 m), and LWC scale-break ($\approx$ 2-5 m). The artificial scales used in this paper are the Landsat pixel ($\approx$ 30 m) and the resolution of Gerber probe (PVM) LWC data (0.04 m). Note that while outer scales L for both vertically homogeneous and variable models are the same, the smallest scales ℓ are quite different; they depend on the maximum number of cascade steps for multidimensional models (11 cascades for 2D models and 7 for 3D models are defined by current limits of our computational power.) As a result, a 1D model goes down to $\ell = 0.04$ m while a 3D model only reaches $\ell = 1$ m.

Finally, as an example, microcanonical properties were prescribed to 1D and 2D models, while canonical properties were prescribed to 3D models. The only purpose of such an example is to show that the radiative transfer results reported in section 4 are valid for both microcanonical and canonical cases. However, a more physically justified 3D model will be microcanonical at large scales and canonical at small scales; this is more like what *Shaw et al.* [1998] see in their direct numerical simulation.

Note that our model atmosphere consists of only one component: inhomogeneous clouds. For simplicity, we assume that no aerosol, no water vapor, and, finally, no surface reflectances are included into our "atmospheric" model.

4. Results

In this section we estimate the effects of sub-mfp variability on cloud radiation by comparing the reflectances of the above models with the ones that are scale-invariant down to the satellite grid-box (20-30 m) and homogeneous below this scale. Our focus will be on the reflectances at nadir, which is the viewing angle of the Landsat satellite. In all calculations solar zenith angles are 0° and 60°.

4.1. *X and X-Y Variabilities*

We start with estimating the effect of x-y variability at different scales. Let

$$I_{3D}(L;r) = \frac{1}{N}\sum_{i=1}^{N} I_i \qquad (10a)$$

with $N = (L/r)^2$; denote the average over the grid-size $L\times L$ nadir radiance I_i computed for the 2D cloud model with a pixel-size $r\times r$; below scale r the model is assumed to be homogeneous. The scale $r = L$ corresponds to the plane-parallel case. We will first compare the results of Independent Pixel Approximation (IPA) and Monte Carlo (MC). While the nadir radiance I_i computed by MC is a solution of the 3D radiative transfer equation [e.g., *Marshak et al.*, 1995b], the IPA radiance [*Cahalan et al.*, 1994]

$$I_{IP}(L;r) = \frac{1}{N}\sum_{i=1}^{N} I_{1D}(\tau_i) \qquad (10b)$$

is just the average over all radiances computed on a pixel-by-pixel basis using 1D radiative transfer.

Figure 5a illustrates both $I_{3D}(L;r)$ and $I_{IP}(L;r)$ as functions of scale r (L = 1000 m $\le r \le$ 2 m = ℓ) for the two solar zenith

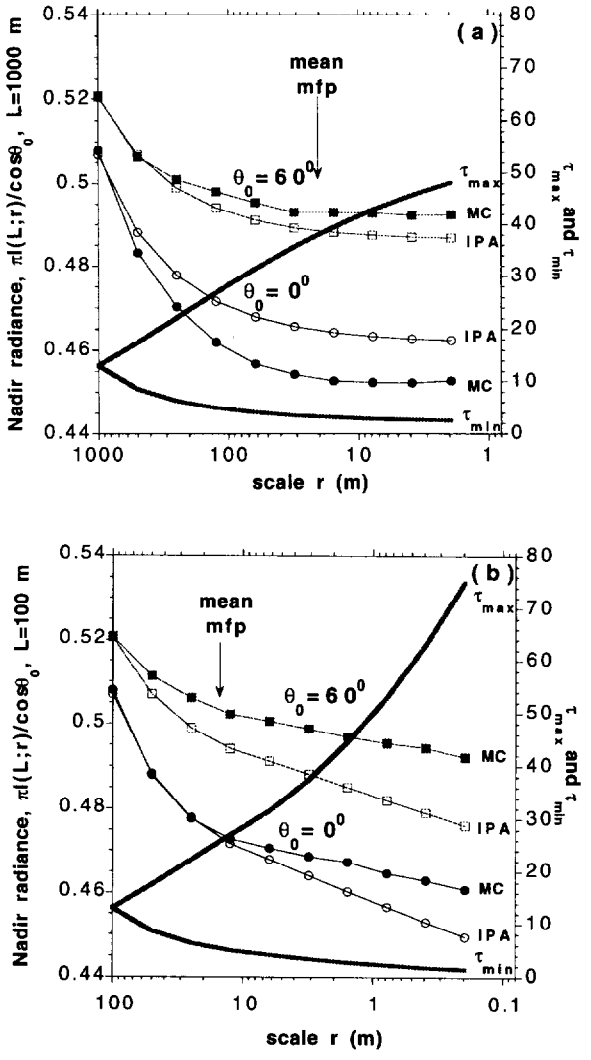

Figure 5. The IPA and MC nadir radiances averaged over scale L versus scale r for x-y variability. Solar angles $\theta_0 = 0°$ and 60°, conservative scattering, Heney-Greenstein phase function with asymmetry parameter $g = 0.843$. Maximal and minimal values of optical depth versus scale illustrate the variability of cloud model. (a) Clouds are simulated by the bounded model only, from L = 1000 m down to ℓ = 2 m. (b) Clouds are simulated by the bounded model from L = 100 m down to 4 m and the singular model from 4 m down to ℓ = 20 cm.

angles: 0° and 60°. The difference between 3D and IPA illustrates the effect of net horizontal fluxes. It is called the IPA bias; for marine Sc the bias is about 1-2% [*Cahalan et al.*, 1994; *Chambers et al.* 1997b]. Note that for sun in zenith,

$$I_{IP} > I_{3D}, \tag{11a}$$

while for a slant illumination

$$I_{IP} < I_{3D}. \tag{11b}$$

The inequality (11a) has been theoretically justified by *Davis* [1992]; for Landsat-derived cloud fields, both cases are discussed by *Chambers et al.* [1997b].

The values $\tau_{max}(r)$ and $\tau_{min}(r)$ are scale-dependent maximal and minimal optical depths, respectively. They represent scales r from L = 1000 m down to ℓ = 2 m; hence for these scales, the bounded model alone is sufficient to simulate the variability of cloud fields. The direct consequence of the "boundnesness" ($\tau_{max}(r) < \infty$) is the saturation of the nadir radiance $I_{3D}(L;r)$ for scales r below photon mean mfp, i.e., for $r \leq 1/\langle\sigma\rangle$ (≈ 20-30 m). To conclude, weak sub-mfp variability does not affect the radiances averaged over scales equal to or larger than photon mfp.

The conclusion will be different if we compare $I_{3D}(L;r)$ and $I_{IP}(L;r)$ for r running from L = 100 m down to ℓ = 0.2 m. In this case, the small-scale variability is simulated with a singular model (Figure 5b). First of all, note that the model becomes unbounded. As a result of strong small-scale fluctuations of optical depth, the radiances keep decreasing with the increase of small-scale variability. However, the decrease of the IPA radiances based on inequality (1) is much faster than the MC ones. The inequality (11a) does not work anymore; for any solar angle, MC radiances are larger than their IPA counterparts.

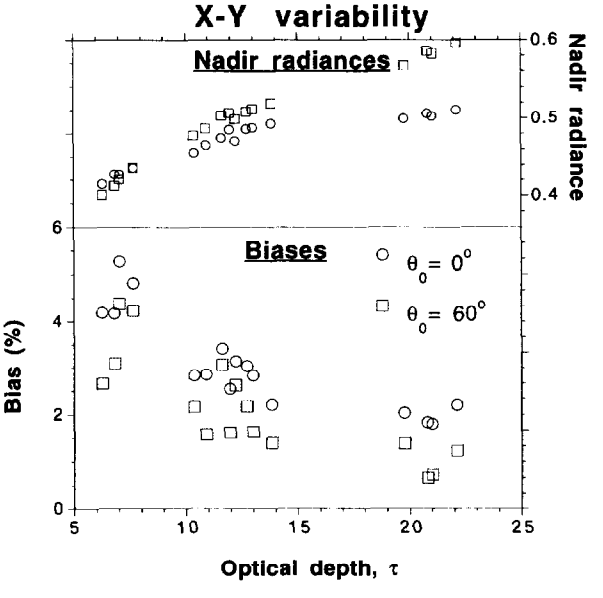

Figure 6. Relative biases for x-y variability. Illumination and scattering conditions are the same as in Figure 5. Biases between models with and without sub-mfp x-y variability for 16 Landsat-size (32×32 m^2) pixels with optical depths simulated by a two-cascade 2D bounded model. Nadir radiances calculated for a model with no variability below 32 m are added for reference.

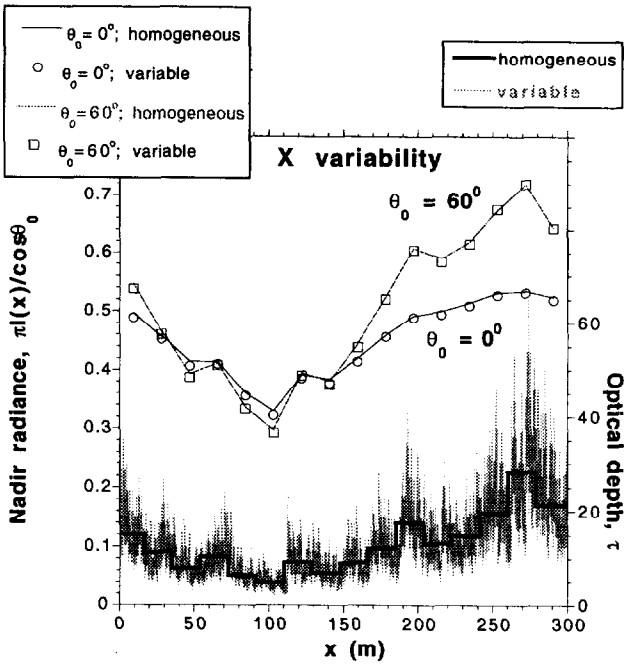

Figure 7. The x variabilities. Illumination and scattering conditions are the same as in Figure 5. Nadir radiances with and without sub-mfp 1D variability for the 16 pixels (≈ 20 m) are shown. Optical depth fields (both homogeneous and variable down to ℓ = 4 cm) are added for reference.

Now let L = 128 m, and r run from L down to ℓ = 6 cm as in Figure 4 (a five cascades bounded model from 128 to 4 m interpolated by a six cascades singular model from 4 m to 6 cm). Altogether we have 4^2 = 16 Landsat-size (32×32 m^2) pixels as represented by a two cascade steps bounded model. Figure 6 illustrates relative biases,

$$B = 100\frac{\left|I - \frac{1}{n}\sum_{i=1}^{n} I_i\right|}{I}(\%), \tag{12}$$

for all 16 pixels and two solar angles. Here I is the nadir radiance calculated for a bounded model with no variability below 32 m; I_i (i = 1,...,n) are the nadir radiances for the smallest resolution of ℓ = 6 cm and $n = (2^9)^2$ = 262144 since nine cascade steps are needed to go from 6 cm up to 32 m. We see that while the average bias is around 3%, for some Landsat-size pixels, B can exceed 5%. As expected, the bias is larger for zenith sun than for a slant illumination. Finally, a larger bias corresponds to pixels with smaller optical depths; this is understandable since the later case is closer to the broken cloud situation, where more radiation is transmitted through clouds and function $I(\tau)$ has a larger gradient.

For better visualization, in Figure 7 we plotted nadir radiances computed for a cloud field with 1D variability only. The optical depth fields are added for reference. We see that the effects of x variability is similar to x-y variability, though it is less pronounced. For example, the averaged bias between homogeneous 20 m pixels and variable down to ℓ = 4 cm is only around 1%. As in the x-y case, the bias is larger for zenith sun and small optical depths. Note that in the 1D case we simulated horizontal variability from L = 300 m down to ℓ = 4 cm using 13 cascades.

The effect of sub-mfp variability on cloud albedo [*Cahalan*, 1989] is different from the effect on nadir radiances. Using the

singular cascade model (see (3a)-(3c)), Cahalan found that the mean albedo becomes insensitive to variations in optical depth on scales smaller than the photon mfp. Our numerical simulations with more realistic cloud models confirm this result: the average smallest-scale (ℓ = 0.04 m) relative albedo bias does not exceed 0.5%. Averaging over 20–30 m brings the difference to negligibly small 0.1%.

For comparison, in our calculations (x variability only, 2^{13} = 8192 pixels and ℓ = 4 cm) the level of pixel-by-pixel Monte Carlo noise was 0.9% for fluxes and 1.5% for radiances. The average over 20 m (500 pixels) fluxes had only 0.04% noise, while radiances had 0.07%. The level of Monte Carlo noise for the case of x-y variability ($2^{2\times11} \approx 4\ 10^7$ pixels and ℓ = 6.25 cm) averaged over 32×32 m^2 was similar (≈ 0.05%), while, on the pixel-by-pixel level, it was 5.2% for fluxes and 8.4% for radiances.

4.2. *X-Z and X-Y-Z Variabilities*

In contrast to the only horizontal variability, x-z and x-y-z cases assume similar fluctuation of the extinction coefficient in both horizontal and vertical directions. As a result, the horizontal pixel-by-pixel variability of optical thicknesses $\tau(x)$ or $\tau(x,y)$ defined respectively by integrals (8b) or (9) is much weaker than the variability of their extinction counterparts. The lower curve in Figure 8 illustrates $\tau(x)$ for a homogeneous below photon mfp $\sigma(x,z)$ (4 cascades) and a variable down to ℓ = 15 cm extinction $\sigma(x,z)$ (11 cascades). We see that the horizontal distribution of optical depth has not been changed much with the increasing variability of $\sigma(x,z)$ (see Figure 3 for illustration of τ_{max}).

The effect of sub-mfp variability of $\sigma(x,z)$ on $I(x)$ is minimal. The average bias B, defined in (12) with $n = 2^7$ = 128 and I_i computed at 15 cm resolution, is less than 0.5% (which is much larger than the level of Monte Carlo noise).

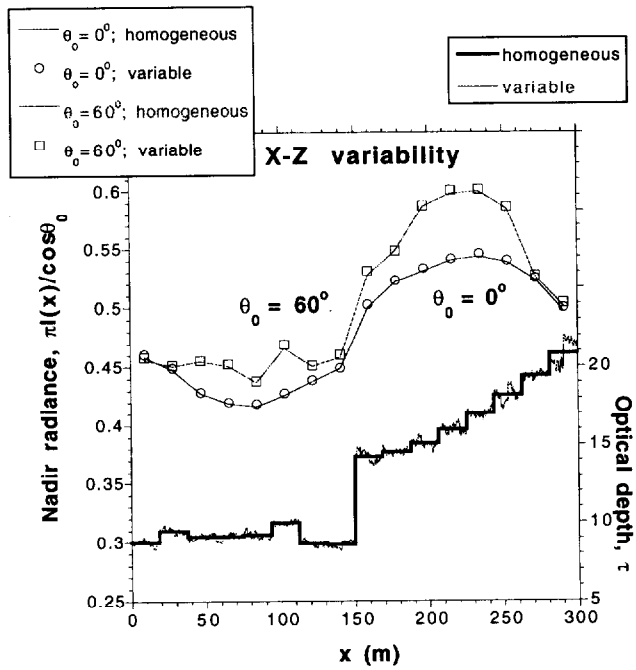

Figure 8. The x-z variability. Scattering conditions are the same as in Figure 5. Nadir radiances with and without sub-mfp variability in $\sigma(x,z)$ for 16 pixels (≈ 20 m) are shown. Optical depths (both homogeneous and variable down to ℓ = 15 cm) are added for reference.

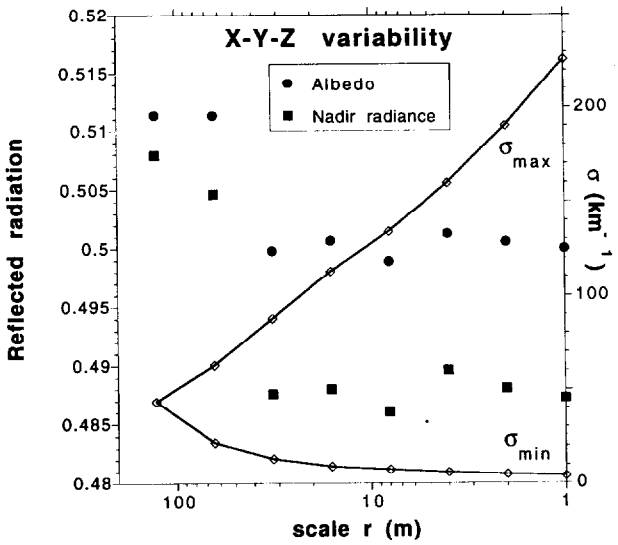

Figure 9. The x-y-z variability. Scattering conditions are the same as in Figure 5. Solar angle $\theta_0 = 0°$. Albedos $R_{3D}(L;r)$ and nadir radiances $I_{3D}(L;r)$ are averaged over three realizations. Scale r changes from L = 128 m down to ℓ = 1 m. Scale-dependent maximal and minimal values of a single realization of $\sigma(x,y,z)$ are shown.

This bias remains unchanged even if the bounded model is extrapolated down to the smallest scale. In contrast to x-y variability, the bias is independent on either solar position or optical depth.

The effect of x-y-z variability on the radiation reflected from clouds is similar to that of x-z variability. However, since our 3D cascade model is canonical and does not conserve liquid water for each realization, the values of both radiances and albedos computed for models with different cascade steps have greater scatter than their microcanonical counterparts. The bold circles and squares in Figure 9 are the values of albedo $R_{3D}(L;r)$ and nadir radiance $I_{3D}(L;r)$, respectively; $I_{3D}(L;r)$ is defined in (10a) with L = 128 m, while $R_{3D}(L;r)$ is its albedo counterpart. Both $R_{3D}(L;r)$ and $I_{3D}(L;r)$ are averaged over three independent realizations of a cloud model and plotted versus scale r: from L = 128 m (plane-parallel case) down to ℓ = 1 m (seven cascade steps). Even after averaging over three realizations, dots are still scattered. Nevertheless, we can see that reflected radiation levels off below photon mfp; therefore sub-mfp variability of the extinction coefficient (see σ_{max} and σ_{min} curves) affects neither albedos nor radiances.

Finally, to make our analysis more robust, for 15 independent realizations of a 3D cloud model with homogeneous and variable structures below 32 m, we test statistically the hypothesis of changing the 32-m-grid radiances as a result of sub-mfp variability in cloud structure. So the hypothesis H_0 states that the average over satellite grid nadir radiance is not changed with sub-mfp variability in cloud liquid water; that is, there is no bias. The alternative hypothesis H_1 reads that there is a bias. It is easy to check that the change is insignificant at 5% level and [e.g., *Korn and Korn*, 1968],

$$t^* = \frac{\langle I_{hom}\rangle - \langle I_{var}\rangle}{s(2/n)^{1/2}} = 0.19 < t = 2.06, \qquad (13)$$

where $\langle I_{hom}\rangle$ and $\langle I_{var}\rangle$ are averaged over n = 15 realizations and 32-m-grid radiances, s is a joint standard deviation, and

2.06 is the value of t for the t-distribution with 28 degrees of freedom at 95% confidence level. Thus hypothesis H_0 is confidently retained.

The validity of the hypothesis H_0 is true not only for conservative scattering but also for absorbing wavelength. Figure 10 shows a scatter plot of nadir radiances for the variable down to 1 m cloud structure versus those of homogeneous below 32 m structures. We used the same 15 independent realizations of a 3D cloud model as for the statistical test above for each of six different single-scattering albedos from the conservative case ($\varpi_0 = 1.00$) down to $\varpi_0 = 0.95$. Concentrated along the diagonal, they justify visually the validity of the H_0-hypothesis for absorbing satellite channels.

To summarize, vertical variability of the extinction field $\sigma(x,y,z)$ substantially smoothes pixel-by-pixel fluctuations of cloud optical thickness $\tau(x,y)$. As a result, the increasing strong variability of $\sigma(x,y,z)$ down to centimeter-scales does not decrease the radiances averaged over satellite-size grids not only for conservative scattering but also for absorbing wavelengths.

5. Discussion

In 1D radiative transfer (i.e., horizontally homogeneous plane-parallel media), the basic transport phenomenology is determined by optical depth τ: the dominant process will be ballistic motion if $\tau \ll 1$ and photon diffusion if $\tau \gg 1$. In a recent study, *Davis et al.* [1998a] propose the norm of gradient of the inverse extinction,

$$\chi(\boldsymbol{x}) = \left|\nabla \frac{1}{\sigma(\boldsymbol{x})}\right|, \tag{14}$$

as a diagnostic tool for the prediction of strong or weak 3D effects around point $\boldsymbol{x}$. Like τ, χ is a nondimensional quantity.

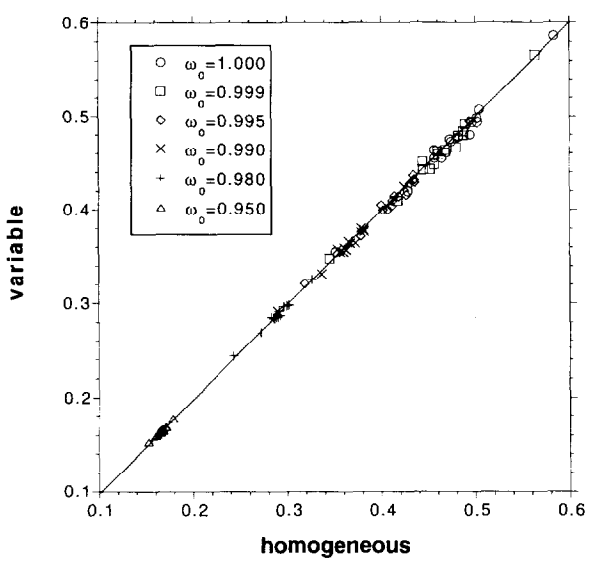

Figure 10. Fifteen independent realizations for a x-y-z geometry. Illumination is the same as in Figure 9. Nadir radiances $I_{3D}(L;r)$ computed for six different single scattering albedos ϖ_0 (1.000, 0.999, 0.995, 0.99, 0.98, and 0.95) and two different cloud structures (homogeneous below 32-m-cube and variable down to 1-m-cube) scatter-plotted against each other. The results are averaged over 128×128 m^2 grid.

1. If $\chi \ll 1$, we have "slow" variability, where $1/\sigma(\boldsymbol{x})$ varies little over a typical photon free path. In this case, we anticipate relatively weak 3D effects that may possibly be modeled by approximate methods that are based on 1D theory [e.g., *Cahalan et al.*, 1994; *Galinsky and Ramanathan*, 1998]. This is the "linear mixing" regime in the theory of stochastic radiative transfer in binary media [*Avaste and Vainikko*, 1974; *Titov*, 1990; *Malvagi et al.*, 1993].
2. If $\chi \gg 1$, we have "fast" variability, where many values of extinction are sampled over a typical photon free path. This case is similar to a homogeneous medium with extinction equal to the average because the cumulative optical distance can be approximated by mean extinction times the path length. This is called the "atomistic mixture" regime in stochastic radiative transfer.

In the random cloud models used in this paper, we go from the former extreme (at large scales) to the latter regime (at small scales), superposed onto the "slow" regime. That is why we find relatively small radiative effects of sub-mfp variability in simulated cloud liquid water.

Another common feature of these two extremes is that mfp is a well-defined quantity. The rigorous definition of photon mfp at point $\boldsymbol{x}_0$ in direction Ω is

$$mfp(\boldsymbol{x}_0,\Omega) = \int_0^\infty t\, \sigma[\boldsymbol{x}(t)]\, \exp\{-\int_0^t \sigma[\boldsymbol{x}(t')]\, dt'\}\, dt \tag{15}$$

where $\boldsymbol{x}(t) = \boldsymbol{x}_0 + t\Omega$. In the case of $\chi \gg 1$, mfp is close to the inverse of mean extinction obtained directly from average column liquid water. In cases where $\chi \ll 1$, extinction fluctuates relatively slowly around a well-defined mean; so global mean extinction is still a very relevant quantity. In particular, it can be used to define a mfp, or at least a global mean mfp, without any detailed knowledge of the radiative transfer. Because of the slow variability, this will be a good approximation to the average of (15) over all $\boldsymbol{x}_0$ and all directions Ω. Indeed in our calculations, the difference between mean values of photon mfp for homogeneous and inhomogeneous cloud structures are less than 0.5% for the large-scale fluctuations ($\chi \ll 1$) and less than 1% for small-scale fluctuations ($\chi \gg 1$).

Returning to (14), strong 3D effects are anticipated only in the intermediate regime where $\chi \approx 1$. In this case, we can predict strong horizontal fluxes and strong departures from exponential free-path distributions. As a result, along with the mean in (15), all other statistical moments are required to describe photon transport.

As a concrete example of $\chi \approx 1$ in meteorology, consider a broken cloud field with around 50/50 cover. The Rayleigh/aerosol atmosphere in which the clouds are embedded is optically thin; consequently, the "out-of-cloud" mfp can be tens to hundreds of kilometers which is several times the scale-height of the atmosphere. So, in sharp contrast with photons "rattling" around (technically "diffusing") inside the clouds, they cover great distances in cloud-cloud, cloud-ground, cloud-space, and ground-space interactions. These long paths will dominate any statistically meaningful mean. In broken clouds, the mfp is therefore at least as large as the intercloud gaps, which can easily exceed the cloud size. Consequently, all variability that is internal to the clouds is arguably sub-mfp. It is important to emphasize this point as a limitation of the present study. This study applies only to stratiform clouds, not so much because the 4-cm resolution data were

collected in marine Sc but because photon mfp is a key radiative transfer parameter only in stratus.

The above photon propagation scenario of incloud diffusion episodes separated by long ballistic intercloud jumps is the starting point of *Davis and Marshak*'s [1997] Lévy-flight model of atmospheric radiation transport. This model, which replaces the standard exponential free path distribution with power-law counterparts, has received some empirical support in recent measurements of total photon path using O_2 A-band spectroscopy [*Pfeilsticker*, 1998].

6. Summary

Because of the lack of cloud liquid water measurements below spatial scales of a photon mfp (≈ 20-30 m in this paper), the problem of how sub-mfp structure affects the interpretation of high-resolution satellite data has been impossible even to address. Thus 3D radiative transfer grid boxes were always assumed homogeneous. Recently, however, the new Particulate Volume Monitor (PVM) instrument [*Gerber et al.*, 1994] was able to measure cloud LWC in marine boundary-layer stratus at unprecedented 4-cm resolution.

Davis et al. [1998b] studied this marine Sc data using a scale-by-scale analysis; they found two distinct scaling regimes separated at a characteristic scale of 2-5 m. While the large-scale behavior was similar to previously analyzed low resolution LWC data with the spectral exponent $\beta_{large} \approx 1.5$, the small-scale fluctuations showed a much larger variability with spectral exponent $\beta_{small} \lesssim 1$. A careful analysis and simulation of the PVM ruled out the possibility that this scale break is an artifact.

This new understanding of sub-mfp variability of cloud liquid water made it possible to generate credible cloud LWC models down to centimeter-scales. Since no high resolution data of optical depth is available, we focused on simulating the extinction field $\sigma(x,y,z)$. As a result, we generated four models of σ: with x, x-y, x-z, and x-y-z variabilities. Each of these models uses bounded cascades [*Cahalan*, 1994] for the large scales, which are then interpolated to small scales using a singular p-model [*Meneveau and Sreenivasan*, 1987] in order to simulate the wavenumber spectrum measured by the PVM. The x and x-y variable models do not have vertical fluctuations. Since the pdf of σ has a long "tail" (roughly lognormal), the same holds for τ. Integrated over z, the x-z and x-y-z models have far less intermittency in the optical depth fields; their pdfs do not have long "tails."

To estimate the effect of sub-mfp variability on 3D radiative transfer through stratus clouds, we compared the results of Monte Carlo computations for several homogeneous "30-m cubes" to their inhomogeneous counterparts, resolved down to centimeter-scales. We found that for vertically homogeneous models (x and x-y variabilities), the horizontal sub-mfp fluctuations of optical depth decrease reflected nadir radiance by 2-3% on average; for some 30-m pixels, with small optical depths, the decrease can exceed 5%. However, as soon as vertical fluctuations are added (x-z and x-y-z variabilities), the effect of sub-mfp inhomogeneity becomes insignificant, with the average bias less than 0.5%. The relative small magnitude of these effects is explained by *Davis et al.*'s [1998a] general phenomenology of 3D radiative transfer.

On the basis of our 3D radiative transfer simulations, stratus cloud models that assume homogeneity below a photon mfp (20-30 m) are quite appropriate for the interpretation of the high-resolution satellite data, and realistic sub-mfp structure in liquid water does not matter much. However, if we were to measure reflected radiation with centimeter- to meter-scale resolution, the retrieval of cloud structure at that resolution would be nearly hopeless.

The results of this paper are restricted to overcast one-layer clouds with flat cloud top and cloud bottom, and relatively small geometrical thickness of 300 m. To extend this study to broken and/or multilayered clouds systems with variable cloud top and different geometrical thicknesses, more data, analyses, models, and computations are required.

Acknowledgments. This work was supported by the Environmental Sciences Division of U.S. Department of Energy (under grant DE-A105-90ER61069 to NASA's Goddard Space Flight Center) as part of the Atmospheric Radiation Measurement (ARM) program. We are grateful to H. Gerber for providing us with the SOCEX data. We thank F. Evans, R. Pincus, and G. Titov for stimulating discussions, and we thank an anonymous reviewer who provided a number of very helpful comments.

References

Albrecht, B. A., D. A. Randall, and S. Nicholls, Observations of marine stratocumulus clouds during FIRE, *Bull. Am. Meteorol. Soc.*, *69*, 618–626, 1988.

Albrecht, B. A., C. S. Bretherton, D. Johnson, W. H. Schubert, and A. S. Frisch, The Atlantic stratocumulus transition experiment — ASTEX, *Bull. Am. Meteorol. Soc.*, *76*, 889–904, 1995.

Avaste, O. A., and G. M. Vainikko, Solar radiation transfer in broken clouds, *Izv. Acad. Sci. USSR Atmos. Oceanic Phys.*, Engl. Transl., *10*, 1054–1061, 1974.

Baker, B., Turbulent entrainment and mixing in clouds: A new observational approach, *J. Atmos. Sci.*, *49*, 387–404, 1992.

Barker, H. W., Solar radiative transfer for clouds possessing isotropic variable extinction coefficient, *Q. J. R. Meteorol. Soc.*, *118*, 1145–1162, 1992.

Barker, H. W., Estimating cloud field albedo using one-dimensional series of optical depth, *J. Atmos. Sci.*, *53*, 2826–2837, 1996.

Barker, H. W., B. A. Wielicki, and L. Parker, A parameterization for computing grid-averaged solar fluxes for inhomogeneous marine boundary layer clouds, 2, Validation using satellite data, *J. Atmos. Sci.*, *53*, 2304–2316, 1996.

Barnsley, M., *Fractals Everywhere*, Academic, San Diego, Calif., 1988.

Byrne, R. N., R. C. Somerville, and B. Subasilar, Broken-cloud enhancement of solar radiation absorption, *J. Atmos. Sci.*, *53*, 878–886, 1996.

Cahalan, R. F., Overview of fractal clouds, in *Advances in Remote Sensing Retrieval Methods*, edited by A. Deepak, H. E. Fleming, and J. S. Theon, pp. 371-388, A. Deepak, Hampton, Va., 1989.

Cahalan, R. F., Bounded cascade clouds: Albedo and effective thickness, *Nonlinear Proc. in Geophys.*, *1*, 156–167, 1994.

Cahalan, R. F., W. Ridgway, W. J. Wiscombe, T. L. Bell, and J. B. Snider, The albedo of fractal stratocumulus clouds, *J. Atmos. Sci.*, *51*, 2434–2455, 1994.

Chambers, L., B. Wielicki, and K. F. Evans, Independent pixel and two-dimensional estimates of Landsat-derived cloud field albedo, *J. Atmos. Sci.*, *54*, 1525–1532, 1997a.

Chambers, L., B. Wielicki, and K. F. Evans, On the accuracy of the independent pixel approximation for satellite estimates of oceanic boundary layer cloud optical depth, *J. Geophys. Res.*, *102*, 1779–1794, 1997b.

Davis, A., Radiation transport in scale-invariant optical media, Ph.D. thesis, McGill Univ., Phys. Dep., Montreal, Que., 1992.

Davis, A., and A. Marshak, Lévy kinetics in slab geometry: Scaling of transmission probability, in *Fractal Frontiers*, edited by M. M. Novak and T. G. Dewey, pp. 63–72, World Sci., River Edge, N.J., 1997.

Davis, A., P. Gabriel, S. Lovejoy, D. Schertzer, and G. Austin, Discrete angle radiative transfer, 3, Numerical results and meteorological applications, *J. Geophys. Res.*, *95*, 11729–11742, 1990.

Davis, A., S. Lovejoy, and D. Schertzer, Radiative transfer in multifractal clouds, in *Scaling, Fractals and Nonlinear Variability in*

Geophysics, edited by. S. Lovejoy and D. Schertzer, pp. 303–318, Kluwer, Acad., Norwell, Mass., 1991a.

Davis, A., S. Lovejoy, and D. Schertzer, Discrete angle radiative transfer in a multifractal medium, *Proc. S.P.I.E.*, Int. Soc. Opt. Eng., *1558*, 37–59, 1991b.

Davis, A., A. Marshak, W. Wiscombe, and R. Cahalan, Multifractal characterizations of nonstationarity and intermittency in geophysical fields: Observed, retrieved, or simulated, *J. Geophys. Res.*, *99*, 8055–8072, 1994.

Davis, A., A. Marshak, W. Wiscombe, and R. Cahalan, Scale-invariance in liquid water distributions in marine stratocumulus, 1, Spectral properties and stationarity issues, *J. Atmos. Sci.*, *53*, 1538–1558, 1996.

Davis, A., A. Marshak, R. Cahalan, and W. Wiscombe, The LANDSAT scale-break in stratocumulus as a three-dimensional radiative transfer effect, implications for cloud remote sensing, *J. Atmos. Sci.*, *54*, 241–260, 1997.

Davis, A., A. Marshak, R. F. Cahalan, and W. J. Wiscombe, Insight into three-dimensional radiation transport processes from diffusion theory, with applications to the atmosphere, in *Proc. of International Symposium on Radiative Transfer*, 1997, edited by P. Mencuc and F. Arinc, Begell House, New York, in press, 1998a.

Davis, A., A. Marshak, H. Gerber, and W. Wiscombe, Horizontal structure of marine boundary-layer clouds from cm- to km-scales, *J. Geophys. Res.*, in press, 1998b.

Gabriel, P., S. Lovejoy, A. Davis, D. Schertzer, and G. Austin, Discrete angle radiative transfer, 2, Renormalization approach for homogeneous and fractal clouds, *J. Geophys. Res.*, *95*, 11717–11728, 1990.

Galinsky V. L., and V. Ramanathan, 3D radiative transfer in weakly inhomogeneous medium, *J. Atmos. Sci.*, in press, 1998.

Gerber, H., B. G. Arends, and A. S. Ackerman, New microphysics sensor for aircraft use, *Atmos. Res.*, *31*, 235–252, 1994.

Knyazikhin, Y., J. Kranigk, R. B. Myneni, O. Panfyorov, and G. Gravenhorst, Influence of small-scale structure on radiative transfer and photosynthesis in vegetation canopies, *J. Geophys. Res.*, *103*, 6133–6144, 1998.

Korn, G. A. and T. A. Korn, 1968: *Mathematical Handbook*, 831 pp., McGraw-Hill, New York, 1968.

Malvagi, F., R. N. Byrne, G. Pomraning, and R. C. J. Somerville, Stochastic radiative transfer in a partially cloudy atmosphere, *J. Atmos. Sci.*, *50*, 2146–2158, 1993.

Mandelbrot, B. B., Intermittent turbulence in self-similar cascades: Divergence of high moments and dimension of the carrier, *J. Fluid Mech.*, *62*, 331–358, 1974.

Mandelbrot, B. B., *Fractals: Form, Chance, and Dimension*, 365 pp., W. H. Freeman, New York, 1977.

Marshak, A., A. Davis, R. F. Cahalan, and W. J. Wiscombe, Bounded cascade models as non-stationary multifractals, *Phys. Rev. E, Stat. Phys. Plasmas Fluids Relat. Interdiscip. Top.*, *49*, 55–69, 1994.

Marshak, A., A. Davis, W. Wiscombe, and G. Titov, The verisimilitude of the independent pixel approximation used in cloud remote sensing, *Remote Sens. Environ.*, *52*, 72–78, 1995a.

Marshak, A., A. Davis, W. Wiscombe, and R. Cahalan, Radiative smoothing in fractal clouds, *J. Geophys. Res.*, *100*, 26247–26261, 1995b.

Meneveau, C., and K. R. Sreenivasan, Simple multifractal cascade model for fully developed turbulence, *Phys. Rev. Lett.*, *59*, 1424–1427, 1987.

Naud, C., D. Schertzer, and S. Lovejoy, Radiative transfer in multifractal atmospheres: Fractional integration, multifractal phase transition and inversion problems, in *Stochastic Models in Geosystems*, edited by W. Woyezinski and S. Molechnsov, pp. 239–267, Springer-Verlag, New York, 1996.

Pfeilsticker, K., First geometrical pathlengths probability density function derivation of the skylight from spectroscopically highly resolving oxygen A-band observations. 2. Derivation of the Lévy-index for the skylight transmitted by midlatitude clouds, *J. Geophys. Res.*, in press, 1998.

Romanova, L. M., Radiative Transfer in a Horizontally Inhomogeneous Scattering Medium, *Izv. Acad. Sci. USSR Atmos. Oceanic Phys.*, Engl. Transl., *11*, 509–513, 1975.

Shaw, R. A., W. C. Reade, L. R. Collins, and J. Verlinde, Preferential concentration of cloud droplets by turbulence: Effects on the early evolution of cumulus cloud droplet spectra, *J. Atmos. Sci.*, *55*, 1965-1976, 1998.

Stephens, G. L., P. M. Gabriel, and S.-C. Tsay, Statistical radiative transport in one-dimensional media and its application to the terrestrial atmosphere, *Transp. Theory Stat. Phys.*, *20*, 139–175, 1991.

Titov, G. A., Statistical description of radiation transfer in clouds, *J. Atmos. Sci.*, *47*, 24–38, 1990.

Zuidema P. and K. F. Evans, On the validity of the Independent Pixel Approximation for the boundary layer clouds observed during ASTEX, *J. Geophys. Res.*, *103*, 6059–6074, 1998.

R. Cahalan, A. Marshak, and W. Wiscombe, NASA Goddard Space Flight Center, Mail Code 913, Greenbelt, MD 20771. (e-mail: cahalan@clouds.gsfc.nasa.gov; marshak@climate.gsfc.nasa.gov; wiscombe@climate.gsfc.nasa.gov)

A. Davis, Space and Remote Sensing Science Group, Los Alamos National Laboratory, P. O. Box 1663 (MS C-323), Los Alamos, NM 87545, (email: adavis@lanl.gov)

(Received November 19, 1997; revised April 23, 1998; accepted May 15, 1998.)